Contract No.:

This manuscript has been authored by Savannah River Nuclear Solutions (SRNS), LLC under Contract No. DE-AC09-08SR22470 with the U.S. Department of Energy (DOE) Office of Environmental Management (EM).

Disclaimer:

Growth of $Cd_{0.9}Zn_{0.1}Te_{1-y}Se_y$ Single Crystals for Room Temperature Gamma-Ray Detection

Joshua W. Kleppinger, *Graduate Student Member, IEEE*, Sandeep K. Chaudhuri, *Member, IEEE,* Utpal N. Roy, *Member, IEEE,* Ralph B. James, *Fellow, IEEE,* and Krishna C. Mandal, *Senior Member, IEEE*

***Abstract*– Quaternary $Cd_{0.9}Zn_{0.1}Te_{1-y}Se_y$ (CZTS) single crystals, a novel room-temperature nuclear radiation detector semiconductor material, have been grown using a modified vertical Bridgman method (VBM) and a travelling heater method (THM). The percentage concentration of selenium in the VBM-grown crystal was 3% and that in the THM-grown crystal was 2%. While the THM Frisch collar detector (4.4 × 4.4 × 10.7 mm^3) produced a highly resolved pulse height spectra (PHS) with a resolution of ~1.06% for 662-keV gamma rays without any correction, the VBM-grown detector (10 × 10 × 2 mm^3) offered a high energy resolution of ~2% after application of a digital biparametric correction. The high-resolution performance of these detectors has been attributed to the addition of Se in the $Cd_{0.9}Zn_{0.1}Te$ (CZT) matrix. *Ab-initio* calculations based on density functional theory (DFT) also confirmed that the addition of Se in the CZT matrix helps to reduce the formation of Te_{Cd} and the Te_{Zn} anti-sites. The VBM-grown crystals were characterized using powder x-ray diffraction (XRD) and energy dispersive x-ray spectroscopy (EDS). While XRD results revealed sharp diffraction peaks confirming the crystalline nature of the grown crystal, the EDS results confirmed the targeted stoichiometry of the elemental composition. The bulk resistivity of the grown crystal was calculated to be ~3 × 10^{10} Ω-cm from current-voltage characteristics recorded at room temperature in a planar configuration, ensuring that the grown CZTS crystals have low dark current as required for detector-grade crystals.**

I. Introduction

Quaternery high-resistivity semiconductor with a stoichiometric composition of the form $Cd_{0.9}Zn_{0.1}Te_{1-y}Se_y$ (CZTS) is a novel high-Z material for room-temperature gamma ray detection [1]-[6]. CZTS has surpassed the well-established $Cd_xZn_{1-x}Te$ (CZT) for some properties relevant to room-temperature compound semiconductor radiation detectors (e.g., crystal growth yield, charge-transport uniformity, and secondary phases). Single crystalline CZTS has been demonstrated to offer a crystal growth yield above 90% [7]-[9], which means that out of the total volume of the grown crystal at least 90% of the volume is of detector grade. The best crystal growth yield reported for CZT amounts to about 33%, which implies that only one-third of the grown crystal volume can be used for detector fabrication [10]. The poor crystal growth yield leads to relatively high manufacturing cost, which eventually leads to higher installation and maintenance cost of spectrometer or imaging systems that use CZT detectors. In comparison, with such high crystal growth yield, CZTS detectors will be undoubtedly offer an economic alternative and potentially provide much better detection performance. CZTS detectors have been demonstrated to offer energy resolution of 0.9% for 662-keV gamma rays [8]. CZTS detectors can thus be considered as a replacement of its ternary predecessor CZT in some applications in the field of homeland security, medical imaging, nuclear material accounting and safeguards, and environmental monitoring [11]-[18].

The primary reason behind obtaining higher energy resolution spectra using CZTS detectors is the significantly lower concentration of tellurium (Te) inclusions and other extended defects compared to that observed in detector-grade CZT single crystals. CZTS single crystal growth has been demonstrated to possess a very low amount of crystal faults such as sub-grain boundaries (SGB) and their networks leading to better charge-transport uniformity. SGB and their networks are primary hosts for Te inclusions. Selenium (Se) is reported to reduce the bulging of the retrograde solidus line near stoichiometry in CZTS preventing the formation of SGB and their networks [19], [20]. The Te inclusions and precipitates pose as the primary trapping centers, which limits the resolution of CZT detectors and creates space-charge buildup in devices. Moreover, the low melting point of Se (221 °C) reduces the generation of Cd vacancies during the growth, which facilitates a reduction of the use of compensating dopants such as indium [19]. The reduced concentration of such dopants is expected to enhance the carrier transport properties [2], [19]. The above observation has also been confirmed by our *ab-initio* defect formation energy calculations and will be discussed at length in a subsequent section. Although the effects of some electrically active defects in CZTS are less pronounced compared to that in CZT, the transport properties and the detector performances of CZTS detectors are still affected by the presence of intrinsic point defects at least to some extent [21]-[23]. In some cases impurities in the Se are an area of concern and must be further investigated due to higher level of impurity content in commercial CdSe source materials, as compared to CdTe.

In the present article, we report the growth conditions and parameters of $Cd_{0.9}Zn_{0.1}Te_{1-y}Se_y$ single crystals using a

Manuscript received January 10, 2021. J. W. Kleppinger, S. K. Chaudhuri, and K. C. Mandal are with the Department of Electrical Engineering, University of South Carolina (UofSC), Columbia, SC 29208, USA, (telephone: (803) 777-2722, e-mail: mandalk@cec.sc.edu). U. N. Roy and R. B. James are with the Savannah River National Laboratory (SRNL), Aiken, SC 29808, USA, (telephone: (803) 725-2362, e-mail: Ralph.James@srnl.doe.gov).

U*of*SC authors acknowledge partial financial support from the DOE Office of Nuclear Energy's Nuclear Energy University Programs (NEUP), Grant No. DE-NE0008662. U. N. Roy and R. B. James acknowledge the support of the U.S. Department of Energy, Office of Defense Nuclear Nonproliferation Research and Development (DNN R&D). U.N. Roy acknowledges partial support from Laboratory Directed Research and Development (LDRD) program from SRNL.

modified vertical Bridgman (VBM) and a traveling heater method (THM). Radiation detectors have been fabricated using both the crystals, which exhibited excellent energy resolution for high energy (662 keV) gamma rays. The grown crystals were characterized in terms of electrical resistivity, tellurium inclusions and precipitates, and radiation detection performance. The related findings are used to devise and implement new growth methodologies that can further improve the detector resolution.

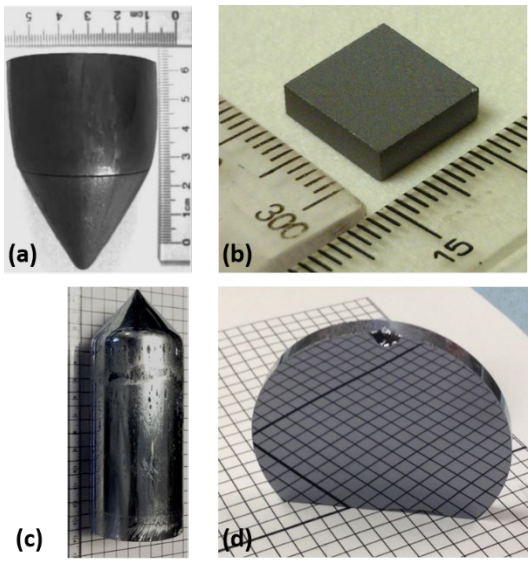

Fig. 1. (a) A 2-inch diameter CZTS boule grown using a VBM. (b) A mechanically polished square wafer cut out from a VBM-grown ingot. (c) A 2-inch diameter CZTS boule grown using the THM. (d) A 2-inch diameter THM-grown CZTS polished wafer.

II. Experimental Methods

VBM growth of CZTS ingots was carried out at U*of*SC by a tellurium solvent method inside a vertical furnace with a modified Bridgman puller in our laboratory. 7N purity Cd, Zn, Te, and Se precursors were weighed in stoichiometric amounts with 5% excess Te, which helps to reduce the growth temperature. The targeted stoichiometry of the ternary compound was $Cd_{0.9}Zn_{0.1}Te_{0.97}Se_{0.03}$. The precursors were sealed under a vacuum of 10^{-6} Torr inside a quartz ampoule (~4-mm wall thickness and ~31-mm inner diameter). Polycrystalline CZTS material was synthesized at a temperature of ~1085 ºC, which was then inserted into a three-zone vertical Bridgman furnace. The furnace was programmed to achieve the desired temperature profile for vertical Bridgman growth. An axial temperature gradient of 2.5 ºC/cm was achieved. The ampoule was moved downward at a constant velocity of 2 mm/hour resulting in a directional solidification. During the axial advancement, the ampoule was constantly rotated at a speed of ~12 rpm. This cycle was repeated three times, and then the furnace was slowly cooled down.

The THM crystals were grown at Brookhaven National Laboratory [7]. The CZTS crystals in the stoichiometry $Cd_{0.9}Zn_{0.1}Te_{0.98}Se_{0.02}$ were synthesized from 6N purity $Cd_{0.9}Zn_{0.1}Te$ and CdSe precursor (pre-synthesized) materials. The precursors were sealed in a conically tipped quartz ampoule under vacuum (10^{-7} Torr) and loaded in a three-zone vertical furnace. The temperatures of the three zones were set to achieve the required temperature gradient near the growth interface. All the growth runs were un-seeded. A very low-speed DC motor was used for lowering the ampoule into the furnace. Different lowering rates from 3 to 5 mm/day were used for the different growth runs, and the temperature gradient near the growth interface was between 10 and 15 ºC/cm. After completion of each growth run, the ingot was cooled at a rate of 100 ºC/day.

Several CZTS crystals were cut out from the grown ingots and were grounded, lapped (down to 1500-grit SiC paper) and polished (down to 0.05-µm alumina powder). To obtain a mirror-finish surface, the hand-polished surfaces of the sectioned pieces were chemo-mechanically polished (CMP) using a 2% bromine-methanol solution (Br_2-MeOH) for 1 minute. Fig. 1 shows photographs of the grown ingots and polished pieces of single crystal wafers.

Powder x-ray diffraction (XRD) pattern of a representative portion of the VBM crystal was collected on a Rigaku Ultima IV D/Max 2100 powder diffractometer using CuK_α radiation ($\lambda = 1.5418$Å). The composition of the ingot was analyzed by energy dispersive x-ray spectroscopy (EDS). EDS mapping data were collected using a high-resolution Tescan Vega 3 SBU scanning electron microscope (SEM) equipped with EDS integration software.

A larger crystal of dimension $4.4 \times 4.4 \times 10.7$ mm^3 was obtained from the THM-grown crystal and was used to fabricate a Frisch collar detector by wrapping with a copper sheath with a proper insulating lining. A planar detector with dimensions $10 \times 10 \times 2$ mm^3 was fabricated from a VBM-grown crystal. Electrical contacts were obtained by sputter coating of gold onto the polished CZTS surfaces.

Current-voltage (*I-V*) characteristics were measured on a Keithley 237 source-measure unit. The analog alpha and gamma ray spectroscopic measurements were carried out using a standard bench-top analog spectrometer with an Amptek A250CF CoolFET pre-amplifier. An NI PCI-5122 high speed and high-resolution digitizer card was used to obtain the digital spectra. A digital data acquisition and analysis program was coded to implement a bi-parametric correction algorithm to obtain high-resolution spectra [24].

III. Results and Discussions

A. Density Functional Theory (DFT) Calculations

To compare the defect formation energy between CZT and CZTS, we calculated the formation energies and transition levels of intrinsic point defects using density functional theory (DFT) on 64 atom supercells using the Vienna ab-initio simulation package (VASP). For the DFT calculations, the zinc concentration was set at 12.5%, and the selenium concentration was taken to be 3.125%. For the CZTS unit cell, we have replaced some of the Te sites with Se randomly in the CZT matrix. Fig. 2(a) shows such a supercell that has been used in the present calculations. The formation energy is defined as the additional energy needed by a defective supercell to form from the non-defective supercell. The formation energy $E_{form}(E_f, q)$ is expressed by the equation below,

$$E_{form}(E_f, q) = E(q) - E_{bulk} - \sum_i n_i(\mu_i + E_i) + q(E_f + E_v) + E_{corr}. \quad (1)$$

where $E(q)$ is the energy of the defective cell, n_i is the number of atoms of species i added or removed, μ_i is the chemical potential of atoms, E_f is the Fermi energy, E_v is the valence band edge energy, and E_{corr} is a correction factor for periodic imaging [25], [26].

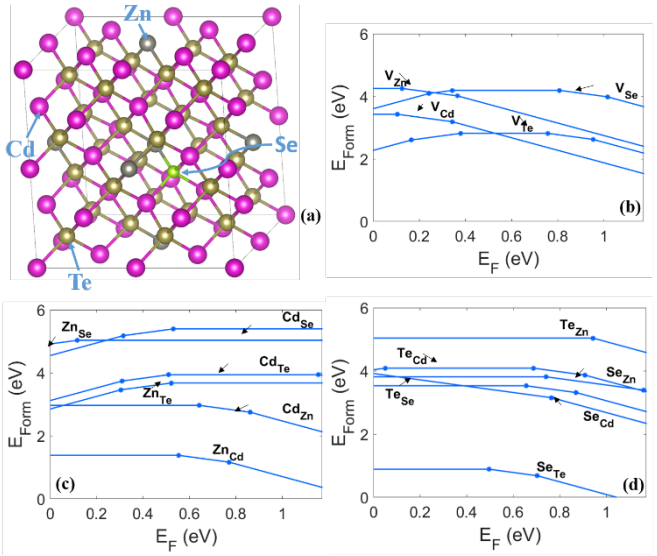

Fig. 2. (a) Primitive supercell of CZTS used for the DFT calculations showing one Te atom replaced by a Se atom in the CZT zinc-blend matrix. (b) – (d) Formation energy plots respectively in CZTS at the CdTe, ZnSe, and ZnTe boundaries.

The transition levels are defined as the Fermi energy where the formation energy plots of the same defect at two different charge states intersect and directly correspond to the trapping of electrons by that particular defect. Fig. 2 (b)-(d) shows the formation energy plots respectively in CZTS at the CdTe, ZnSe, and ZnTe boundaries. The calculations showed that for the CZTS crystal there is an increase of at least 1 eV in the formation energy of Te_{Cd} and the Te_{Zn} anti-sites confirming the notion that the addition of Se in the CZT crystals helps to reduce the formation of point defects, in particular replacement of cadmium and zinc sites by tellurium.

B. Material Characterization

Fig. 3 shows the powder XRD and EDS of the VBM-grown CZTS crystal. The XRD spectrum shown in Fig. 3 (a) of the grown crystal exhibits sharp diffraction peaks confirming the crystallinity of the grown ingot. As there was no reference to the stoichiometric composition for $Cd_{0.9}Zn_{0.1}Te_{0.97}Se_{0.03}$ in the JCPDS library, the crystal planes corresponding to the XRD peaks were identified by comparing them with those in the XRD spectra of CdZnTe (JCPDS 00-053-0552). All the peaks observed in the present study have been noticed in CZT crystals with slight offset in the peak positions. The offsets in the peak positions are thought to be due to the inclusion of Se in the CZT matrix. The atomic ratio of Cd/Te was calculated to be 0.88 from the EDS shown in Fig. 3(b), which is close to the expected value of 0.947 for the stoichiometric condition. The atomic ratio of (Cd+Zn)/(Te+Se) was calculated to be 0.903.

Fig. 4 (a) shows a high magnification infrared (IR) transmission image of the as-grown THM crystal. The image barely shows the presence of Te inclusions or precipitates. In CZT, large concentrations of Te inclusions with a diameter bigger than 10-μm act as potential charge trapping and recombination centers leading to permanent charge loss [27]-[30].

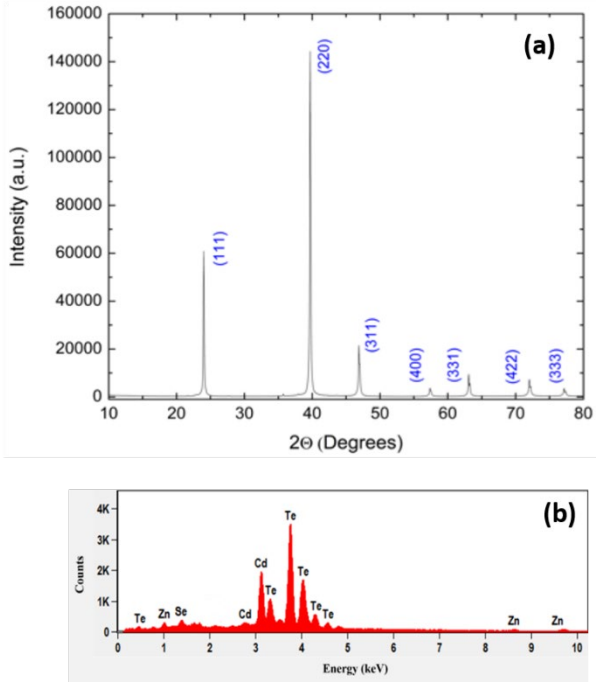

Fig. 3. (a) X-ray diffractogram showing the single crystalline nature of the VBM-grown CZTS crystal. (b) EDX pattern showing the elemental peaks obtained from a polished CZTS detector.

Fig. 4 (b) shows an IR transmission image of the VBM-grown CZTS crystals. Although the density of the Te inclusions appears to be larger in comparison to the THM-grown crystals, the size of the Te inclusions were less than 10 μm.

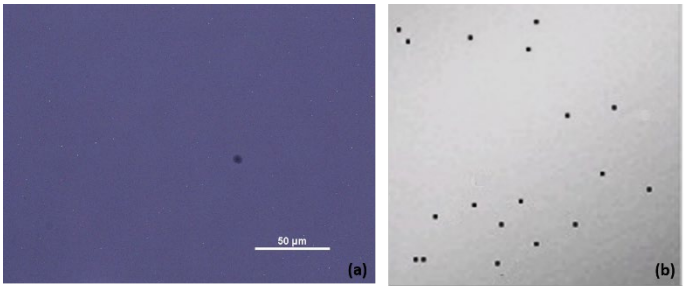

Fig. 4. IR transmission images obtained for the THM (a) and VBM (b) grown crystals.

C. Detector Characterization

Fig. 5 shows the *I-V* characteristics of both the detectors recorded at room-temperature. The bulk resistivity was calculated to be ~3×10^{10} Ω-cm and ~1×10^{10} Ω-cm in the

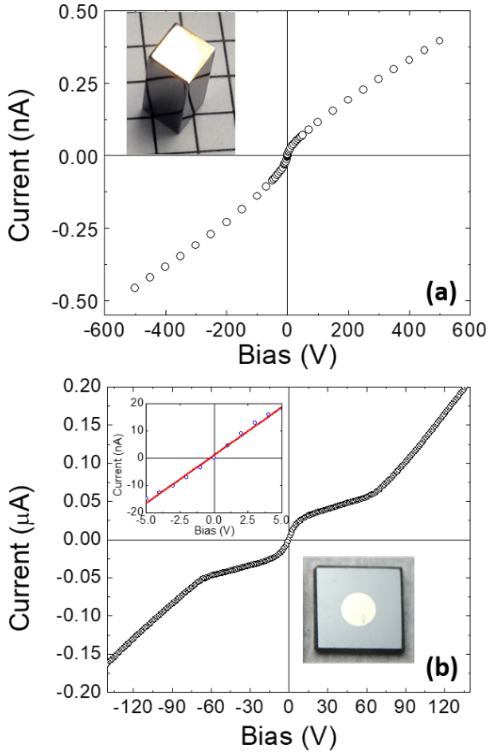

Fig. 5. Current-voltage characteristics recorded at room-temperature in a Frisch-grid configuration for (a) $4.4 \times 4.4 \times 10.7$ mm^3 THM-grown crystal and planar (b) $10 \times 10 \times 2$ mm^3 VBM-grown crystal. Inset graph in (b) shows the low range *I-V* curve for the resistivity determination. Also shown are the photographs of the actual detectors in planar configuration used for the measurements.

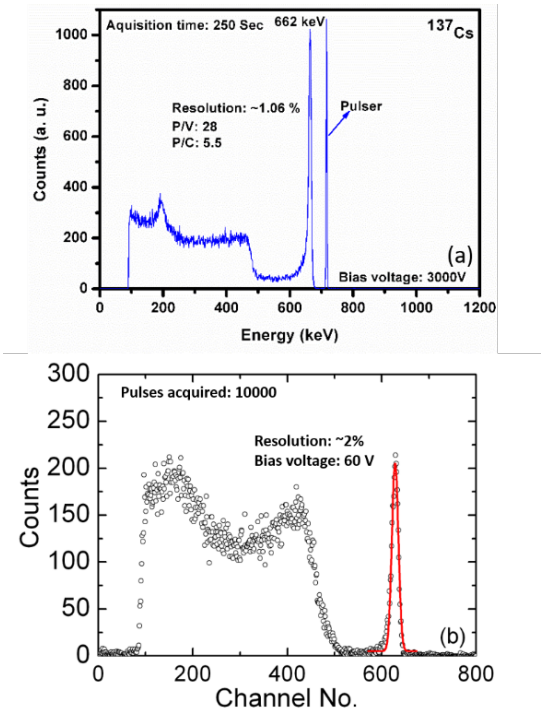

Fig. 6. Pulse height spectra obtained from (a) Frisch collar detector fabricated on the THM-grown crystal and (b) a planar detector fabricated on the VBM-grown crystal after applying a digital correction. No digital correction was used for the Frisch collar detector.

THM- and VBM-grown crystals, respectively.

Figs. 6 (a) & (b) show the pulse-height spectrum (PHS) obtained from the Frisch grid detectors fabricated from the THM and the planar detectors fabricated from the VBM-grown crystals respectively when exposed to a ^{137}Cs source. Both the detectors exhibited high resolution PHS with photo-peaks neatly resolved from the Compton background. The PHS obtained from the THM Frisch grid detector showed an energy resolution of 1.06% for the 662-keV gamma rays. The PHS from the planar detector showed an energy resolution of 2% after the application of a digital correction scheme. The performance of the planar VBM detector was affected by hole trapping, which has been confirmed from the bi-parametric correlation plot shown in Fig. 7.

Bi-parametric plots correlate the rise-time and the pulse-height of each pre-amplifier pulse resulting from each gamma ray-detector interaction in a 2-D plot – x-axis being the pulse-height and y-axis being the rise-times. In an ideal case of complete charge collection (i.e., where no charge trapping occurs), photoelectric events resulting from the interaction of gamma rays having the same energy appear as a vertically straight band of events in the bi-parametric plots. In the case of trapping and recombination, usually these bands incline towards the left, indicating that the pulses with longer rise-times register lower pulse-heights. The longer pulses in CZT or CZTS crystals originates from the slower hole movement because of multiple trapping and detrapping of the hole traps. Most of these charge carriers recombine before reaching the collecting electrodes, thereby depositing partial charges and hence registers lower pulse heights. Fig. 7 (a) shows such a bending of the 662-keV photopeak events. Fig 7 (b) shows the same bi-parametric plot but after applying a digital correction scheme. The correction scheme brings the affected events to the correct coordinates in the event of no charge loss. The pulse height spectra shown in Fig. 7 (b) has been regenerated from the corrected bi-parametric plot.

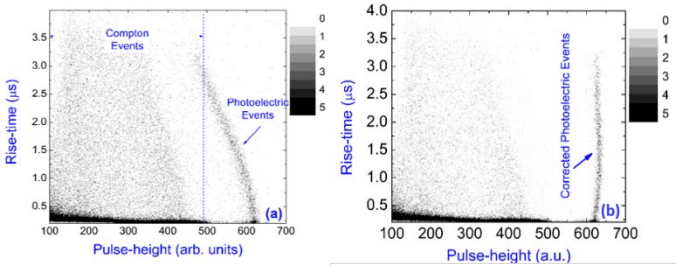

Fig. 7. (a) Bi-parametric correlation plots obtained from the planar detector fabricated on a VBM-grown crystal. The inclination of the 662-keV gamma ray photoelectric events confirms that hole trapping limited the detector resolution. (b) Corrected bi-parametric plot obtained after application of a digital correction scheme, which rectifies the effect of trapping and incomplete charge collection for slow-moving holes.

IV. Conclusion

Radiation detectors for high-energy gamma rays have been fabricated from $Cd_{0.9}Zn_{0.1}Te_{1-y}Se_y$ (CZTS) single crystals, an emerging room-temperature nuclear radiation detector material. Using DFT calculations, it was established that addition of Se

in the CZT matrix helps to prohibit formation of Te inclusions/precipitates and anti-sites. CZTS single crystals were grown using two different methods viz., a vertical Bridgman method (VBM) and a travelling heater method (THM). Both the crystals showed bulk resistivity on the order of 10^{10} Ω-cm at room temperature based on *I-V* measurements in a planar geometry. The THM-grown crystals showed the presence of tellurium inclusions and precipitates in much lower concentrations compared to the VBM-grown crystals. A Frisch collar detector was fabricated from the THM-grown crystal, which showed a very high energy-resolution of 1.06% for 662-keV gamma rays as determined from the as-recorded pulse-height spectrum. A planar detector was fabricated from the VBM crystal, which offered a good energy resolution of 2% for 662-keV with the application of a digital bi-parametric correlation-based correction scheme. The better energy resolution of the THM-grown detector is mostly related to the lower concentration of Te inclusions/precipitates as revealed by IR transmission images. Further studies are underway to investigate whether the difference in the percentage of Se in the two crystals is linked to the observed difference in the size and concentration of Te inclusions or whether it is the inherent nature of the crystal growth technique that controls the formation of Te inclusions.

REFERENCES

[1] U. N. Roy, G. S. Camarda, Y. Cui, R. Gul, A. Hossain, G. Yang, J. Zazvorka, V. Dedic, J. Franc and R. B. James, "Role of selenium addition to CdZnTe matrix for room-temperature radiation detector applications," *Sci. Rep.,* vol. 9, no. 1, pp. 1620-1-1620-7, Feb. 2019.

[2] A. Yakimov, D. Smith, J. Choi and S. Araujo, "Growth and characterization of detector-grade CdZnTeSe by horizontal Bridgman technique," *Proc. SPIE,* vol. 1114, pp. 11141N-1–111141N-7, Sep. 2019.

[3] S. K. Chaudhuri, M. Sajjad, J. W. Kleppinger and K. C. Mandal, "Correlation of space charge limited current and γ-ray response of $Cd_xZn_{1-x}Te_{1-y}Se_y$ room-temperature radiation detectors," *IEEE Electron Dev. Lett.,* vol. 41, no. 9, pp. 1336-1339, Sept. 2020.

[4] S. U. Egarievwe, U. N. Roy, E. O. Agbalagba, B. A. Harrison, C. A. Goree, E. K. Savage and R. B. James, "Optimizing CdZnTeSe Frisch-grid nuclear detector for gamma-ray spectroscopy," *IEEE Access,* vol. 8, pp. 137530-137539, Jul. 2020.

[5] S. K. Chaudhuri, M. Sajjad, J. W. Kleppinger and K. C. Mandal, "Charge transport properties in CdZnTeSe semiconductor room-temperature γ-ray detectors," *J. Appl. Phys.,* vol. 127, pp. 245706-1 - 245706-8, Jun. 2020.

[6] S. K. Chaudhuri, M. Sajjad and K. C. Mandal, "Pulse-shape analysis in $Cd_{0.9}Zn_{0.1}Te_{0.98}Se_{0.02}$ room-temperature radiation detectors," *Appl. Phys. Lett.,* vol. 116, pp. 162107-1-162107-5, Apr. 2020.

[7] U. N. Roy, G. S. Camarda, Y. Cui, R. Gul, G. Yang, J. Zazvorka, V. Dedic, J. Franc and R. B. James, "Evaluation of CdZnTeSe as a high-quality gamma-ray spectroscopic material with better compositional homogeneity and reduced defects," *Sci. Rep.,* vol. 9, no. 1, pp. 7303-1-7303-7, May 2019.

[8] U. N. Roy, G. S. Camarda, Y. Cui and R. B. James, "High-resolution virtual Frisch grid gamma ray detectors based on as-grown CdZnTeSe with reduced defects," *Appl. Phys. Lett.,* vol. 114, pp. 232107-1-232107-4, Jun. 2019.

[9] U. N. Roy, G. S. Camarda, Y. Cui and R. B. James, "Characterization of large-volume Frisch grid detector fabricated from as-grown CdZnTeSe," *Appl. Phys. Lett.,* vol. 115, pp. 242102-1–242102-4, Dec. 2019.

[10] U. N. Roy, S. Weiler, J. Stein, Y. Cui, M. Groza, V. Buliga and A. Burger, "Zinc mapping in THM grown detector grade CZT," *J. Cryst. Growth,* vol. 347, no. 1, pp. 53-55, May 2012.

[11] T. E. Schlesinger, J. E. Toney, H. Yoon, E. Y. Lee, B. A. Brunett, L. Franks and R. B. James, "Cadmium zinc telluride and its use as a nuclear radiation detector material," *Mater. Sci. Eng. R Rep.,* vol. 32, pp. 103-189, Apr. 2001.

[12] A. E. Bolotnikov, K. Ackley, G. S. Camarda, Y. Cui, J. F. Eger, G. De Geronimo, C. Finfrock, J. Fried, A. Hossain, W. Lee, M. Prokesch, M. Petryk, J. L. Reiber, U. N. Roy, E. Vernon, G. Yang and R. B. James, "High-efficiency CdZnTe gamma-ray detectors," *IEEE Trans. Nucl. Sci.,* vol. 62, no. 6, pp. 3193-3198, Dec. 2015.

[13] S. Del Sordo, L. Abbene, E. Caroli, A. M. Mancini, A. Zappettini and P. Ubertini, "Progress in the development of CdTe and CdZnTe semiconductor radiation detectors for astrophysical and medical applications," *Sensors,* vol. 9, no. 5, pp. 3491-3526, May 2009.

[14] K. C. Mandal, R. M. Krishna, P. G. Muzykov and T. C. Hayes, "Fabrication and characterization of $Cd_{0.9}Zn_{0.1}Te$ Schottky diodes for high resolution nuclear radiation detectors," *IEEE Trans. Nucl. Sci.,* vol. 59, no. 4, pp. 1504-1509, Jul. 2012.

[15] C. G. Wahl, W. R. Kaye, W. Wang, F. Zhang, J. M. Jaworski, A. King, Y. Andy Boucher and Z. He," The Polaris-H imaging spectrometer," *Nucl. Instrum. Meth. Phys. Res. A,* vol. 784, pp. 377-381, Jun. 2015.

[16] M. Streicher, D. Goodman, Y. Zhu, S. Brown, S. Kiff and Z. He, "Fast neutron detection using pixelated CdZnTe spectrometers," *IEEE Trans. Nucl. Sci.,* vol. 64, no. 7, pp. 1920-1926, May 2017.

[17] M. Sajjad, S. K. Chaudhuri, J. W. Kleppinger and K. C. Mandal, "Growth of large-area $Cd_{0.9}Zn_{0.1}Te$ single crystals and fabrication of pixelated guard-ring detector for room-temperature γ-ray detection," *IEEE Trans. Nucl. Sci.,* vol. 67, no. 8, pp. 1946-1951, Aug. 2020.

[18] L. Abbene, F. Principato, G. Gerardi, A. Buttacavoli, D. Cascio, M. Battelli, N. S. Amadè, P. Seller, M. C. Veale, O. Fox, K. Sawhney, S. Zanettini, E. Tomarchio and A. Zappettini, "Room-temperature x-ray response of cadmium–zinc–telluride pixel detectors grown by the vertical Bridgman technique," *J. Synchrotron Radiat.,* vol. 27, no. 2, pp. 319-328, Mar. 2020.

[19] S. Hwang, H. Yu, A. E. Bolotnikov, R. B. James and K. Kim, "Anomalous Te Inclusion Size and Distribution in CdZnTeSe," *IEEE Trans. Nucl. Sci.,* vol. 66, no. 11, pp. 2329-2332, Oct. 2019.

[20] U. N. Roy, A. E. Bolotnikov, G. S. Camarda, Y. Cui, A. Hossain, K. Lee, W. Lee, R. Tappero, G. Yang, R. Gul and R. B. James, "High compositional homogeneity of $CdTe_xSe_{1-x}$ crystals grown by the Bridgman method," *APL Mater.,* vol. 3, pp. 026102-1-026102-7, Feb. 2015.

[21] R. Gul, U. N. Roy, G. S. Camarda, A. Hossain, G. Yang, P. Vanier, V. Lordi and R. B. James, "A comparison of point defects in $Cd_{1-x}Zn_xTe_{1-y}Se_y$ crystals grown by Bridgman and travelling heater methods," *J. Appl. Phys.,* vol. 121, pp. 125705-1-125705-7, Mar. 2017.

[22] M. Rejhon, J. Franc, V. Dědič, J. Pekárek, U. N. Roy, R. Grill and R. B. James, "Influence of deep levels on the electrical transport properties of CdZnTeSe detectors," *J. Appl. Phys.,* vol. 124, pp. 235702-1-235702-6, Dec. 2018.

[23] M. Rejhon, V. Dědič, L. Beran, U. N. Roy, J. Franc and R. B. James, "Investigation of deep levels in CdZnTeSe crystal and their effect on the internal electric field of CdZnTeSe gamma-ray detector," *IEEE Trans. Nucl. Sci.,* vol. 66, no. 8, pp. 1952-1958, Aug. 2019.

[24] S. K. Chaudhuri, K. J. Zavalla, R. M. Krishna and K. C. Mandal, "Biparametric analyses of charge trapping in $Cd_{0.9}Zn_{1.0}Te$ based virtual Frisch grid detectors," *J. Appl. Phys.,* vol. 113, pp. 074504-1-074504-6, Feb. 2013.

[25] S. B. Zhang, S. H. Wei, A. Zunger and H. Katayama-Yoshida, "Defect physics of the $CuInSe_2$ chalcopyrite semiconductor," *Phys. Rev. B,* vol. 57, no. 16, pp. 9642-9656, Apr. 1998.

[26] Freysoldt, J. Neugebauer and C. G. van de Walle, "Fully ab initio finite-size corrections for charged-defect supercell calculations," *Phys. Rev. Lett.,* vol. 102, no. 1, pp. 016402-1-016402-4, Jan. 2009.

[27] G. A. Carini, A. E. Bolotnikov, G. S. Camarda, W. G. Wright, R. B. James and L. Li, "Effect of Te precipitates on the performance of CdZnTe detectors," *Appl. Phys. Lett.,* vol. 88, no. 14, pp. 143515-143517, Apr. 2006.

[28] R. M. Krishna, P. G. Muzykov and K. C. Mandal, "Electron beam induced current imaging of dislocations in $Cd_{0.9}Zn_{0.1}Te$ crystal," *J. Phys. Chem. Solids*, vol. 74, no. 1, pp. 170-173, Jan. 2013.

[29] S. K. Chaudhuri, R. M. Krishna, K. J. Zavalla, L. Matei, V. Buliga, M. Groza, A. Burger and K. C. Mandal, "$Cd_{0.9}Zn_{0.1}Te$ Crystal Growth and Fabrication of Large Volume Single-Polarity Charge Sensing Gamma Detectors," *IEEE Trans. Nucl. Sci.*, vol. 60, no. 4, pp. 2853-2858, Aug. 2013.

[30] P. J. Sellin, A. W. Davies, S. Gkoumas, A. Lohstroh, M. E. Özsan, J. Parkin, V. Perumal, G. Prekas and M. Veale, "Ion beam induced charge imaging of charge transport in CdTe and CdZnTe," *Nucl. Instrum. Meth. Phys. Res. B,* vol. 266, no. 8, pp. 1300-1306, Apr. 2008.